

**Structural and chemical effects on EELS  $L_{3,2}$  ionization edges in Ni-based intermetallic compounds**

P. L. Potapov

*EMAT, University of Antwerp, RUCA, Groenenborgerlaan 171, B-2020 Antwerp, Belgium*

S. E. Kulkova

*Institute of Strength Physics and Materials Science, Akademicheskoy 2/1, 634021 Tomsk, Russia*

D. Schryvers and J. Verbeeck

*EMAT, University of Antwerp, RUCA, Groenenborgerlaan 171, B-2020 Antwerp, Belgium*

(Received 4 May 2001; published 22 October 2001)

EELS  $L_{3,2}$  ionization edges in several Ni-based intermetallic compounds have been studied and interpreted in terms of the distribution of electrons in the valence  $d$  bands. It is demonstrated that the integral EELS cross sections change only slightly upon the formation of intermetallic compounds and, therefore, the charge transfer between atoms is negligible. On the other hand, changes in the energy loss near edge fine structure (ELNES) of the Ni  $L_3$  edge can be readily detected, indicating an important redistribution of  $d$  electrons at the Ni site. Full-potential linearized augmented-plane-wave calculations of the density of states (DOS) and simulations of the Ni  $L_3$  edge EELS profiles show that these changes correspond to a hybridization between the Ni  $d$  band and  $d$  bands of the alloying elements. In contrast, structural transformations in the investigated intermetallic compounds do not significantly affect the ELNES as the typical energy resolution of EELS is not sufficient to track the slight difference in the DOS between various structural modifications of intermetallic compounds.

DOI: 10.1103/PhysRevB.64.184110

PACS number(s): 79.20.Uv, 71.20.Be, 71.20.Eh, 71.20.Gj

**I. INTRODUCTION**

In previous decades, electron energy loss spectroscopy (EELS) and x-ray absorption spectroscopy (XAS) were recognized as powerful tools to probe the electronic structure in solids. Both methods provide information about electronic states around the selected atoms, although XAS typically shows a much better energy resolution than EELS. However, the advantage of EELS over XAS is its very high spatial resolution down to the nanometer level,<sup>1</sup> allowing the study of not only extended crystals but also microstructures, precipitates, grain boundaries, internal interfaces, and other lattice defects.<sup>2</sup> Still, such specific applications heavily rely on a full understanding of EELS data from perfect crystals, i.e., a proper correlation of the observed changes in spectra with changes in the local electronic structure. The latter changes can be the result of, e.g., local compositional or structural differences (the structural effect on EELS spectra should not be ignored *a fortiori*).

In this paper the focus is on the  $L_{3,2}$  ionization edges of transition metals (TM), which appear due to the transitions of excited inner  $p_{1/2}$  ( $L_2$  edge) and  $p_{3/2}$  ( $L_3$  edge) electrons to the empty valence states. The study of the integral EELS cross section (i.e., total number of counts in a particular energy window) at these edges yields information on the total charge around a given element, whereas the details of the electron loss near edge structure (ELNES) relate to the actual density of states (DOS) distribution above the Fermi level. The dipole selection rule allows the transition into the  $d$  or  $s$  final states only, and as the probability of a transition to  $s$  states is much smaller than that to  $d$  states, only the  $d$  band needs to be considered. Due to the fact that this  $d$  band is very narrow, specific sharp peaks known as white lines are generally found at the  $L_{3,2}$  edges. A number of EELS studies

have related the changes in the  $L_{3,2}$  edges to changes in the valence  $d$  bands of the transition metals. In particular, Leapman *et al.*<sup>3</sup> investigated a range of  $3d$  metals and concluded that the measured and calculated width of the white lines decreases with increasing atomic number as it correlates with the filling up of the  $3d$  band. Later Pearson *et al.*, in an experimental study of a series of  $3d$  and  $4d$  transition metals,<sup>4,5</sup> have shown that the white line intensities decrease nearly linearly with the occupancy of the  $d$  band in each series. Further, Botton *et al.*<sup>6</sup> and later Muller *et al.*<sup>7</sup> have demonstrated that the observed changes of ELNES upon the formation of TM aluminides can be successfully reproduced by augmented-plane-wave (APW) calculations, and these changes reflect clearly the bonding trends between Al and TM atoms.

However, ELNES cannot always be interpreted as a fingerprint of the DOS distribution above the Fermi level as many-body effects under the influence of the core hole in the  $2p$  state cause a redistribution of intensity in the  $L_{3,2}$  edges.<sup>8,9</sup> In late TM elements such as Ni and Cu, etc., where the  $d$  band is almost full and successfully screens the unoccupied states from the core hole, a single-particle description is still appropriate.<sup>10</sup> On the other hand, in early TM elements with few  $d$  electrons many-body effects are important and the ELNES shape cannot be directly related to the DOS distribution.<sup>11,12</sup> Another drawback is that EELS measures the empty electronic states while only the occupied states are important for the bonding. Recently, however, Muller<sup>13</sup> has suggested a simple model that relates the unoccupied DOS distribution to the bonding trends in metals, greatly simplifying the interpretation of EELS. The model is based on two key assumptions: the absence of many-body effects and the absence of charge transfer among atoms upon the formation of compounds.

In the present work the changes in the experimental EELS  $L_{3,2}$  edges of transition metals upon the formation of intermetallic compounds are investigated and the amount of charge transfer among atoms is estimated. *Ab initio* calculations have been performed in order to relate the observed changes in the experimental spectra to the redistributions of the DOS in the valence  $d$  bands. All examined intermetallic compounds contain Ni, which was chosen as a probe element because (i) the splitting between Ni  $L_2$  and  $L_3$  edges is significant (while in earlier  $3d$  metals, these can overlap), which allows us to track the fine features in the ELNES, and (ii) many-body effects are expected to be small in a Ni atom.<sup>6</sup> The focus is on stoichiometric 50:50 compounds with transition metals (NiMn and TiNi), although one Ni compound with an  $sp$  metal (NiAl) is also examined mainly for comparison with earlier results by Botton *et al.*<sup>6</sup> and Muller *et al.*<sup>7</sup> Also, the environment of Ni atoms in TiNi was adjusted by introducing Cu or Hf atoms. In ternary  $\text{Ti}_{50}\text{Ni}_{25}\text{Cu}_{25}$  [referred to as Ti(NiCu)] and  $\text{Ti}_{25}\text{Hf}_{25}\text{Ni}_{50}$  [referred to as (TiHf)Ni] compounds, Cu or Hf atoms randomly replace half of the Ni or Ti atoms, respectively, without a significant change of the crystal structure<sup>14,15</sup> so that the effect of mixed atomic environments on the ELNES of a Ni atom can be studied. All investigated compounds in their high-temperature modification show the  $B2$  structure, although, at room temperature, they can transform martensitically into  $L1_0$  in NiMn (Ref. 16),  $B19'$  in TiNi (Ref. 17) and (TiHf)Ni (Ref. 18), and  $B19$  in Ti(NiCu) (Ref. 15). The availability of several crystal modifications allow us to separate the effects of the crystal structure and chemical environment on the EELS spectra.

The paper is organized in the following way. Section II describes the measurements and treatments of the EELS spectra and the details of the *ab initio* calculations. As the quantification of the spectra is largely affected by plural scattering, special attention has been paid to establish an accurate procedure for deconvolution and normalization enabling us to properly compare the intensity profiles in different compounds. In Sec. III A, it is demonstrated that the integral cross sections of the  $L_{3,2}$  edges change only slightly upon the formation of compounds, which means the absence of an appreciable charge transfer among atoms. The ELNES or fine structure of the Ni  $L_{3,2}$  edges, however, changes noticeably, indicating relevant changes in the bonding. Section III B demonstrates that full-potential linearized-augmented-plane-wave (FLAPW) calculations can reasonably well reproduce the ELNES changes observed as a result of the formation of intermetallic compounds and during structural transformations. In Sec. IV, the effect of chemical and structural factors on EELS spectra is discussed, emphasizing the priority of the first one. Further, FLAPW calculations show that the observed changes in ELNES of NiMn- and TiNi-based compounds are caused by hybridization between  $d$  Ni and  $d$  TM bands. Finally, a maximum for the value of the charge transfer in several intermetallic compounds is estimated and it is concluded that the model introduced by Muller<sup>13</sup> is adequate for the present intermetallic systems.

## II. METHODS

### A. Experimental procedures

Disk-shaped samples of all investigated materials were thinned down to electron transparency by double jet electropolishing followed by a light ion milling. Details of the preparation of the original material (in bulk or melt-spun shapes) can be found in earlier publications.<sup>14,15,19</sup> The finishing ion-milling procedure was applied in order to remove a thin oxide layer introduced by the chemical electropolishing without noticeably affecting the metallic surface. The absence of an appreciable amount of oxygen in the samples was verified and confirmed by EELS. The energy-loss experiments were carried out on a Philips CM30 transmission electron microscope equipped with a post-column Gatan imaging filter. The microscope uses a Shottky field emission gun operating at 300 kV, resulting in a good signal to background ratio in EELS. The spectra were collected in diffraction mode with a camera length of 175 mm, which corresponds to a collection semiangle of 3.5 mrad. The grains under study were oriented close to a  $\langle 100 \rangle$  zone for NiAl and a  $[101]$  zone for Ni-, NiMn-, and TiNi-based intermetallic compounds. Perfect zone orientations were avoided in order to eliminate possible channeling that could complicate the interpretation of the inelastic scattering events.<sup>20</sup> The estimated energy resolution varies from 1.1 eV in the region of the zero-loss peak to 1.6 eV in the region of 800–1000 eV loss. Spectra were recorded with a correction for the detector dark current and gain variation. The background was modeled as a power law using a window of about 10 eV in width just before the Ni  $L_3$  edge and then subtracted from the edge region. The thickness of the samples varied between 30 and 50 nm (i.e., about half of the inelastic mean free path in these materials), resulting in noticeable effects of plural scattering convoluting core and valence excitations. To correct for plural scattering, the core-loss spectra were deconvoluted by the Fourier-ratio method<sup>21</sup> using low-loss spectra collected from the same regions and under the same diffraction conditions except for a reduced illumination intensity. As the deconvolution procedure was the major potential source of errors, special attention was paid to establish the procedure of switching from a core-loss to low-loss collection, which involves a sharp reduction of the incident beam intensity. Finally, a good reproducibility of the deconvoluted spectra is in favor of the usefulness of the applied procedure. Due to a systematic energy drift of the gun, the accuracy of the absolute energy measurements was about 2 eV while the variation of the threshold position in different compounds is expected to stay below 1 eV. Thus, for better comparison of the post-edge fine structure, the experimental spectra were aligned to match the same threshold position defined as the inflection point at the  $L_3$  threshold.

### B. Computational details

Self-consistent band structure calculations were performed using the WIEN 97 implementation<sup>22,23</sup> of the FLAPW method<sup>24</sup> with the local-density and generalized-gradient approximations<sup>25</sup> for the exchange-correlation po-

tential. The core states were treated in a fully relativistic fashion. The scalar-relativistic calculations were performed for the valence band states and the  $3s$  and  $3p$  states of Ni, Mn, Ti, and Cu atoms and the  $5s$  and  $5p$  states of the Hf atom. The wave functions within the muffin-tin (MT) spheres were expanded in spherical harmonics with the angular momenta up to  $l=10$ . Additional local orbital extensions were used to avoid linearization errors. Nonspherical contributions to the charge density and the potential within the muffin-tin spheres were considered up to  $l_{\max}=4$ . In the interstitial region plane waves with reciprocal lattice vectors up to  $|G|=10$  were included. The electron energy spectrum was calculated at 165, 168, 128, and 144  $\mathbf{k}$  points in the irreducible part of the Brillouin zone for  $B2$ ,  $B19$ ,  $B19'$ , and  $L1_0$  structures, respectively. The self-consistency is considered to be achieved when the total energy variation from iteration to iteration does not exceed  $10^{-5}$  Ry. The lattice parameters for NiMn were taken from Potapov *et al.*<sup>26</sup> and for TiNi from Kudoh *et al.*<sup>27</sup> In the case of ternary TiNi-based alloys, our own x-ray data for lattice parameters and atomic positions were used, which are slightly different from previous data of Nam *et al.*<sup>28</sup> and Potapov *et al.*<sup>14</sup> For each compound, the same radius of the muffin-tin sphere of Ni equal to 2.3 a.u. was used. In the case of Ni and NiMn, spin polarization was included in calculations and the large  $\mathbf{k}$ -point sets were tested to ensure good convergence of the magnetic moment. The electron-energy-loss spectra were calculated according to the formalism described by Nelhiebel *et al.*<sup>29</sup> and Hebert-Souche *et al.*<sup>30</sup> accounting both for orientation of the crystal and for integration over the collection angle of the experiment.

### III. RESULTS

#### A. Experiment

Figure 1 shows the experimental results of the background subtracted and deconvoluted Ti, Mn, Ni, and Cu  $L_{3,2}$  edges in the investigated intermetallic compounds (except for those including Hf). As a reference, the same edges in pure metals are also measured for Ni and Cu. As has been reported previously,<sup>3</sup> the ratio between the  $L_3$  and  $L_2$  white line integrated intensities deviates from the value of 2:1, which is expected on the basis of  $2j+1$  degeneracy of the initial  $2p_{1/2}$  and  $2p_{3/2}$  core states. This ratio was found to be 0.75, 3.6, 3.0, and 1.7 for Ti, Mn, Ni, and Cu edges, respectively (and irrespective of the actual compound), which is close to the numbers measured by Leapman *et al.*<sup>3</sup> in pure metals (0.7, 3.1, and 1.7 for Ti, Ni, and Cu, respectively). A possible explanation of this anomaly is a breakdown of the  $j$ - $j$  coupling due to an exchange mechanism.<sup>3</sup> The comparison of the Ni  $L_3$  to  $L_2$  ratio in various Ni-containing compounds with that in pure Ni did not reveal any noticeable difference with the value of 3.0. The vertical scale of the experimental spectra is always measured in relative units because of difficulties in the calibration of sample thickness and beam intensity. For a quantitative comparison, all spectra obtained on different samples have been scaled using the normalization procedure suggested by Pearson *et al.*<sup>4,5</sup> This

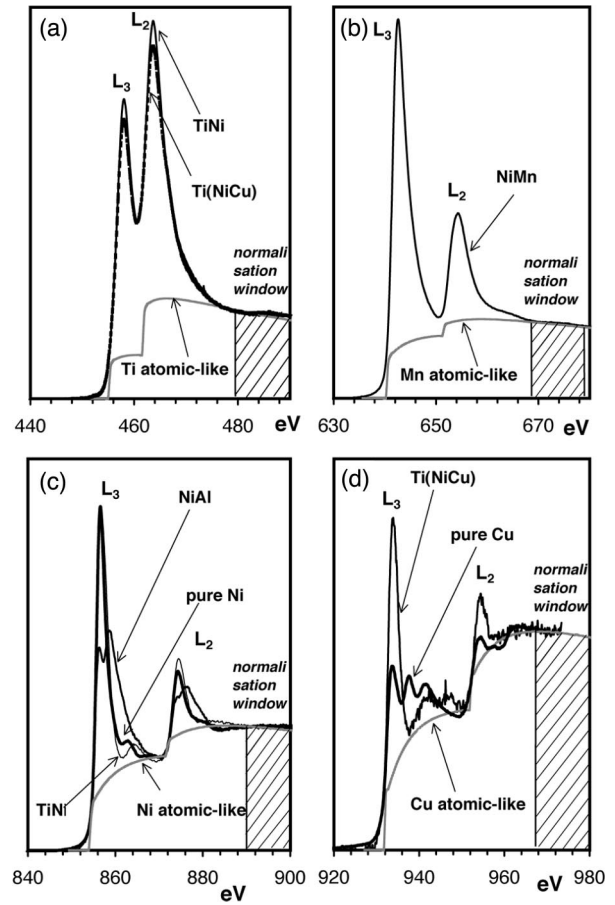


FIG. 1. Examples of background subtracted, deconvoluted, and normalized: (a) Ti, (b) Mn, (c) Ni, and (d) Cu experimental  $L_{3,2}$  edges in different intermetallic compounds. For each atom, the calculated Hartree-Slater atomiclike cross section is also plotted. The area in excess of the calculated atomiclike cross section indicates the amount of  $d$  holes in the material. For Ni and Cu, the experimental spectra of the pure metal are also incorporated.

procedure is based on the assumption that the ELNES fine structure quickly fades out when increasing the energy above the threshold value. Thus, the level of scattering well beyond the threshold will always arrive at the same value in different materials, irrespective of the environment of an atom. There is, however, a discrepancy in determining the position of the normalization window, as Pearson *et al.*<sup>5</sup> place it at 50 eV beyond the  $L_3$  threshold while Muller *et al.*<sup>31</sup> place it at 30 eV beyond the  $L_3$  threshold. The choice is crucial as, on the one hand, the window should lay well beyond the white lines (which are affected strongly by the solid state bonding effects), while on the other hand, placing the window too far beyond the threshold may cause significant errors in the procedure of the background subtraction (as the usually used power law interpolation is valid only in a limited energy range). In the present experiments, it is noticed that the strong variation of ELNES lasts until approximately 15 eV beyond each of the  $L_3$  and  $L_2$  thresholds. Therefore, a window of 10 eV in size was placed at 18 eV after the  $L_2$  threshold and all measured cross sections were normalized to this window.

TABLE I. Experimental  $L_{3,2}$  cross sections integrated in the range  $L_3 - 3$  eV to  $L_2 + 18$  eV and normalized to the window placed at  $L_2 + 18$  eV to  $L_2 + 28$  eV. To extract the information about bound states, the atomiclike cross sections were calculated within the same ranges.

Ionization edge	Material	Normalized total cross sections	Normalized total cross sections reduced by an atomiclike cross section
Ti $L_{3,2}$ edge	Ti atomiclike	2.330	
	$B19'$ TiNi	5.294	2.964
	$B19$ Ti(NiCu)	5.029	2.699
	$B19'$ (TiHf)Ni	4.994	2.664
Mn $L_{3,2}$ edge	Mn atomiclike	2.612	
	$L1_0$ NiMn	5.269	2.657
Ni $L_{3,2}$ edge	Ni atomiclike	2.787	
	Ni fcc metal	3.834	1.047
	$B2$ NiAl	3.882	1.095
	$L1_0$ NiMn	3.858	1.071
	$B19'$ TiNi	3.893	1.106
	$B2$ TiNi	3.922	1.135
	$B19$ Ti(NiCu)	3.889	1.102
	$B19'$ (TiHf)Ni	3.842	1.055
Cu $L_{3,2}$ edge	Cu atomiclike	2.744	
	Cu fcc metal	3.114	0.370
	$B19$ Ti(NiCu)	3.182	0.438

Furthermore, as demonstrated by Müller and Wilkins,<sup>32</sup> any spectrum can be factorized into the atomiclike and solid-state contributions. The former term is analogous to the scattering from the core shell of a free atom to the free-electron continuum. The second term is specific for each solid and proportional to the density of the band states. The atomiclike term shows a smooth energy dependence while the solid-state one varies rapidly near the threshold, yielding the experimentally observed ELNES details. Well above the threshold, however, the solid-state contribution becomes negligible and overall scattering is defined by the atomiclike term. Following the approach described by Leapman *et al.*<sup>33</sup> and Ahn and Rez,<sup>34</sup> we have calculated<sup>35</sup> the atomiclike cross sections for each atom in the Hartree-Slater approximation and added those to Fig. 1 using the same normalization window as for the experimental curves. The part of the experimental cross section area exceeding the calculated atomiclike ones can be considered as a measure of the number of holes in the  $d$  bands. A similar procedure (although less physically established) was used by Pearson *et al.*<sup>5</sup> for evaluating the amount of  $d$  holes in pure metals. Table I lists the total experimental cross sections integrated in the range from  $L_3 - 3$  eV to  $L_2 + 18$  eV and those subtracted from the atomiclike term. The estimated amount of  $d$  holes decreases along the line  $\text{Ti} \rightarrow \text{Mn} \rightarrow \text{Ni} \rightarrow \text{Cu}$  and qualitatively agrees with data by Pearson *et al.* for the pure metals<sup>5</sup> Ni and Cu. In contrast, the number of holes around a Ni atom changes only slightly upon the formation of intermetallic compounds. Comparing with pure fcc Ni, it increases only 2% in  $L1_0$

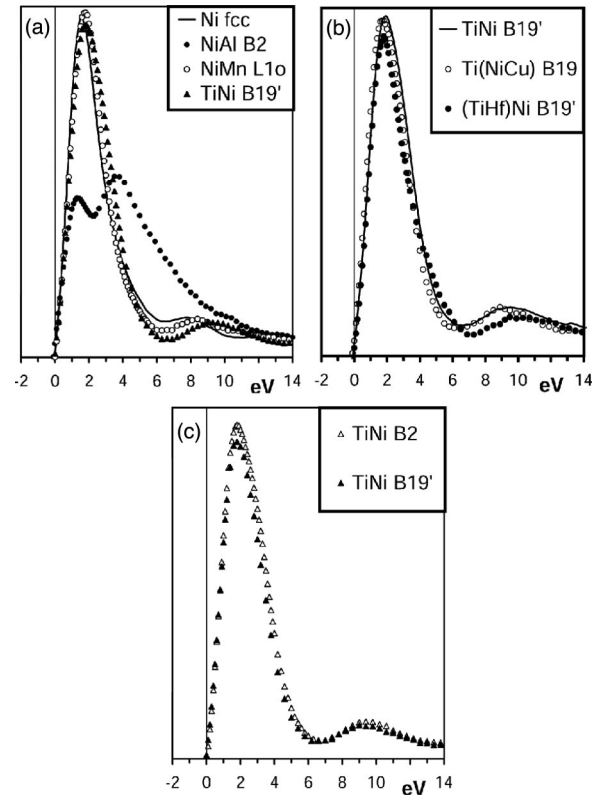


FIG. 2. Experimental measures of the fine ELNES of the Ni  $L_3$  edge in different intermetallic compounds. The vertical line represents the edge threshold.

NiMn, 4% in  $B2$  NiAl, and 6% in  $B19'$  TiNi. All these numbers are within or near the limit of experimental error, which is 1.5% in measuring the total cross section and comes to 5% after subtracting the atomiclike term. Similarly, the amount of  $d$  holes around a Ti atom varies only slightly in different Ti-containing compounds. As for Cu, when comparing the spectra in Fig. 1(d) it looks as if the cross section of the fcc Cu  $L$  edge changes significantly on the formation of  $B19$  Ti(NiCu) intermetallic compound as the latter shows a sharp white line while pure Cu has a smoother threshold. However, quantitative analysis shows that the white line in  $B19$  Ti(NiCu) is formed by the fusion of a number of smaller peaks in the pure Cu spectrum into a single strong peak only slightly increasing the total cross section.

Aside from the total cross section integrated over the particular energy window, the fine details of the ELNES can be carefully examined in the Ni  $L_3$  edge, which shows an appropriated intensity level and large energy separation between the  $L_3$  and  $L_2$  thresholds. It is noted that the ELNES in the range of 15 eV after the thresholds are similar for the  $L_3$  and  $L_2$  edges. The only difference is that the intensity variations behind the  $L_2$  edge are less resolved due to the lower intensity of the  $L_2$  edge and the superposed tails from the  $L_3$  edge. Thus, the ELNES was analyzed in the narrow region between  $L_3$  and  $L_2$  thresholds, where it is believed to represent the general features observed after both Ni  $L_2$  and  $L_3$  edges. Figure 2(a) shows this region with the spectra vertically scaled as described above, allowing the compari-

son of the white line intensity and shape. Those intensities are similar for all examined compounds except for NiAl, which shows a splitting of the major white line into two peaks of reduced height, as has been reported previously.<sup>6,7</sup> The white lines are narrow in Ni and NiMn and wider in TiNi. The latter correlates well with XAS data reported by Fuggle *et al.*<sup>36</sup>. Another noticeable feature of the ELNES is a small but well-resolved secondary peak located around 8 eV after the threshold in pure Ni and NiMn but which is shifted to the right in TiNi and NiAl.

The spectra of the ternary TiNi-based compounds are shown in Fig. 2(b) in comparison with the binary TiNi one. The ELNES of Ti(NiCu) looks very similar to that of TiNi, probably due to the fact that the nearest-neighbor environment for the Ni atom is not changed (assuming Cu atoms replace Ni atoms, they appear on the second coordination sphere around a Ni atom). In the case of (TiHf)Ni, however, half of the Ti atoms in the first coordination sphere around Ni are replaced by Hf, resulting in visible changes in the ELNES. Indeed, the shape of the white line becomes sharper near the top and wider near the bottom while the secondary peak shifts to the right compared with the reference binary B19' TiNi.

Figure 2(c) compares the ELNES of two TiNi samples with composition close to 50:50 and only differing in 0.5 at.%. Due to the strong composition dependency of the transformation temperature in the Ti-Ni system, one of the samples shows the B19' structure while the other one contains the B2 structure. However, no appreciable differences between the spectra of B19' TiNi and B2 TiNi, neither in the width of the white line nor in the position of the secondary peak, are observed. In the case of NiMn, the cubic B2 modification is only stable at temperatures higher than 1000 K, which limits the experimental EELS data to the tetragonal L1<sub>0</sub> NiMn modification. Thus, the effect of the structural transformation on the ELNES in NiMn has been studied by *ab initio* calculations only as described in Sec. III B.

### B. Calculations

The calculated total and *d* partial DOS for the investigated compounds as well as for reference pure Ni are shown in Fig. 3. The shapes of the DOS for Ni and NiAl [Fig. 3(a)] are very similar to those in the work of Botton *et al.*<sup>6</sup> and Muller *et al.*,<sup>7</sup> who used other programming codes for their calculations. As expected, the total DOS is formed mainly by *d* states of the transition metals, with Ni *d* states dominating at the lower energies and Mn(Ti) states dominating at the higher energies. It is worth noting that, in both TiNi and NiMn [Fig. 3(b)], the position of the minor *d* Ni DOS peaks above  $E_F$  coincide with the strong *d* Ti or *d* Mn peaks, respectively. The same coincidence of the *d* Ni and *d* TM peaks is observed in the ternary (TiHf)Ni and Ti(NiCu) compounds [Fig. 3(c)]. As this feature could be affected by the choice of the MT sphere radii, the DOS for binary TiNi was recalculated for the various ratios of the Ni and Ti MT spheres. The calculations demonstrate that the overall shape of the partial DOS remains virtually unchanged although the absolute values of each partial DOS depend strongly on the

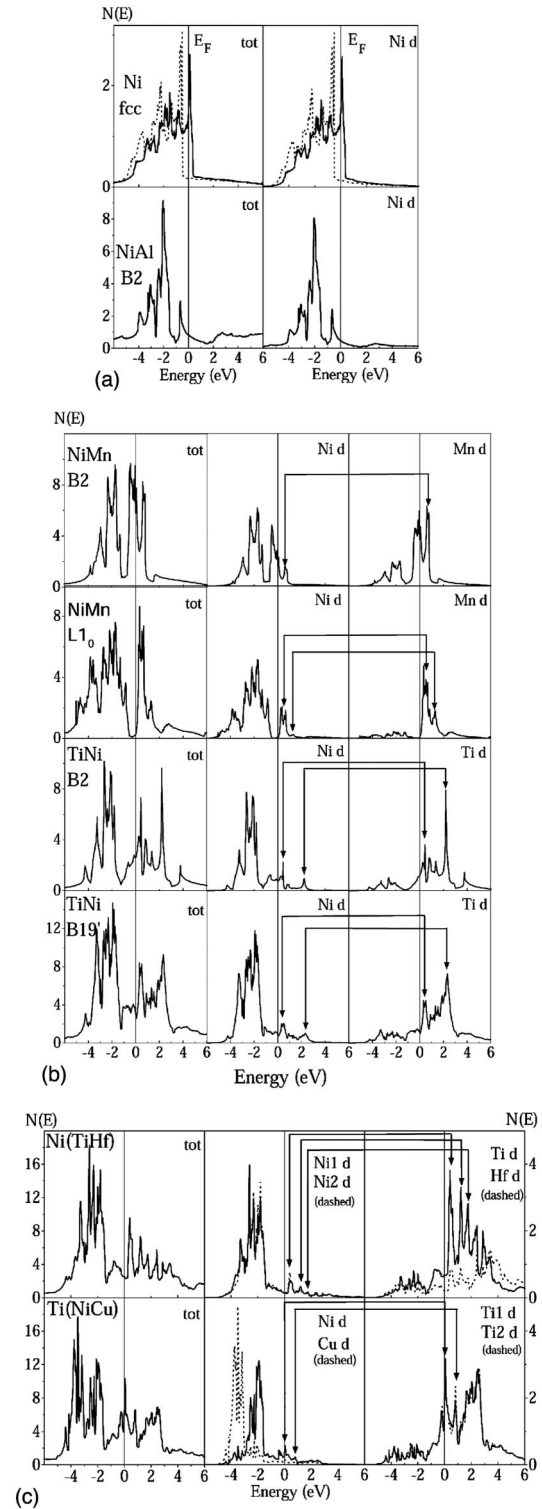


FIG. 3. Calculated density of states for pure (a) Ni, NiAl, (b) TiNi, NiMn, and (TiHf)Ni, and (c) Ti(NiCu). The total DOS are given on the left while the partial *d* Ni and *d* TM contributions are shown on the right. In some structures, Ni or Ti atoms can have two slightly different environments denoted as Ni 1, Ni 2 and Ti 1, Ti 2. Notice the coinciding peaks in *d* Ni and *d* TM states, indicated by bridging arrows in (b) and (c).

TABLE II. FLAPW valence charge in the muffin-tin spheres and in the interstitial region ( $I$ ), expressed in electron/atom. Results obtained by Muller *et al.* (Ref. 7) using the MT sphere radii of 2.31, 2.38, and 2.30 a.u. for Ni, Ni<sub>3</sub>Al, and NiAl, respectively, are indicated with an asterisk. In the present calculations, a fixed MT radius of 2.3 a.u. was used to allow for a comparison between different compounds ( $M$  stands for Mn, Ti, or Al, depending on the compound).

Material	Ni $s$	Ni $p$	Ni $d$	Ni $f$	$M s$	$M p$	$M d$	$M f$	$I$
Ni	0.448	0.423	8.226	0.048					0.854
Ni*	0.463	0.446	8.226	0.031					0.834
B2 NiMn	0.366	0.294	8.133	0.014	0.170	0.142	4.639	0.008	1.617
L1 <sub>0</sub> NiMn	0.448	0.410	8.268	0.024	0.349	0.339	4.930	0.029	1.102
B2 TiN	0.518	0.394	8.243	0.012	0.224	0.237	1.773	0.021	1.289
B19' TiNi	0.525	0.436	8.233	0.016	0.223	0.235	1.792	0.023	1.259
B2 NiAl	0.434	0.440	8.405	0.012	0.616	0.763	0.173	0.031	1.063
B2 NiAl*	0.435	0.444	8.378	0.016	0.618	0.759	0.177	0.025	1.074 <sup>a</sup>
L1 <sub>2</sub> Ni <sub>3</sub> Al	0.478	0.470	8.385	0.025	0.683	0.773	0.204	0.035	0.808
L1 <sub>2</sub> Ni <sub>3</sub> Al*	0.502	0.508	8.423	0.028	0.706	0.820	0.220	0.039	0.707

<sup>a</sup>Reference 45.

chosen MT radius. Thus, the observed coincidence of the  $d$  Ni and  $d$  TM peaks is not an artifact of the choice of the basis set but rather indicates the formation of common electronic states between Ni and TM sites. This, in analogy with  $sp$ - $d$  hybridization, could be interpreted as a hybridization between  $d$  Ni and  $d$  Ti(Mn) states.

To estimate the charge transfer on the formation of intermetallic compounds, the partial valence charges at the MT spheres were also calculated (see Table II). For a comparison with earlier results by Muller *et al.*,<sup>7</sup> the ordered L1<sub>2</sub> Ni<sub>3</sub>Al compound is also included. As the total charge in the component spheres is sensitive to the sphere size, the same radius of the MT spheres (2.3 a.u.) was used in all investigated compounds. In the case of Ni, Ni<sub>3</sub>Al, and NiAl, despite the different calculation methods and different radii of the MT spheres used, both our results and those of Muller *et al.* indicate that the charge redistribution in NiAl compared with pure Ni is smaller than 0.2 electrons/atom. As seen from Table II, the formation of NiMn and TiNi compounds causes an even smaller change of the number of  $d$  electrons in the Ni MT sphere.

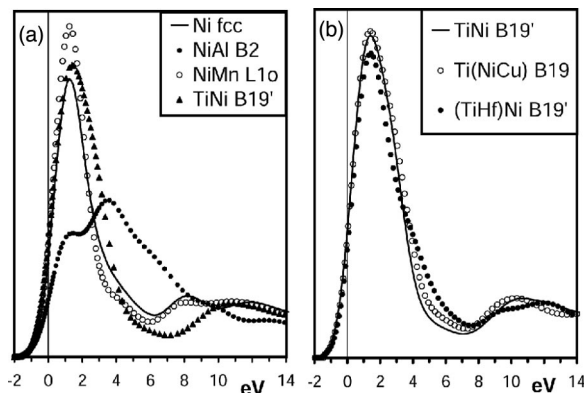


FIG. 4. Calculated Ni  $L_3$  EELS edges for different intermetallic compounds. As a reference, the ELNES of (a) pure Ni or (b) binary TiNi are also displayed.

Figure 4(a) shows the calculated Ni  $L_3$  edge in Ni, NiAl, NiMn, and TiNi. The calculations reproduce well the ELNES profiles and positions of characteristic features found in the experiment, as seen in Fig. 2(a). In particular, in both calculations and experiments, the white lines are the widest in TiNi and the narrowest in pure Ni. As was mentioned above, NiAl shows a splitting of the white line and the calculated splitting value (2.1 eV) is close to the observed value of  $2.3 \pm 0.1$  eV. Also in agreement with experiment is the changing position of the secondary peak, which in pure Ni occurs around 8 eV and is shifted to the higher energy in TiNi. The calculation, however, slightly overestimates this shift as the secondary peak for TiNi results in 10.5 eV instead of the experimentally observed value of 9.5 eV. The weak shoulder detected experimentally in NiAl at 10 eV is also reproduced in the calculations. In the case of NiMn, the calculation reproduces the experimental position of the secondary peak although its shape is slightly different from the experimental one. The additional small peaks at around 12 eV in the calculation of pure Ni are not observed experimentally. This feature probably arises from the linearization of the Hamiltonian matrix in the FLAPW method, which is strictly valid in the center of the valence band but, in principle, can fail for the unoccupied states far above the Fermi level. Rez *et al.*<sup>37</sup> estimated that the departure from the linear interpolation would appear between 10 and 20 eV above the Fermi level, which means that linear methods will do well only just above the threshold, and these additional peaks could thus be considered as an artifact of the approximations in the theory.

The calculated Ni  $L_3$  edges for the ternary TiNi-based intermetallic compounds [Fig. 4(b)] also demonstrate reasonable agreement with experiment [see Fig. 2(b)]. The ELNES profiles of Ti(NiCu) and TiNi remain close to one another while the white line in (TiHf)Ni shows a sharpened maximum at the top and a widening near the bottom. As in the experiment, the secondary peak in (TiHf)Ni is slightly shifted to the right from that in TiNi, although the calculated shape of this peak is more asymmetric than experimentally observed.

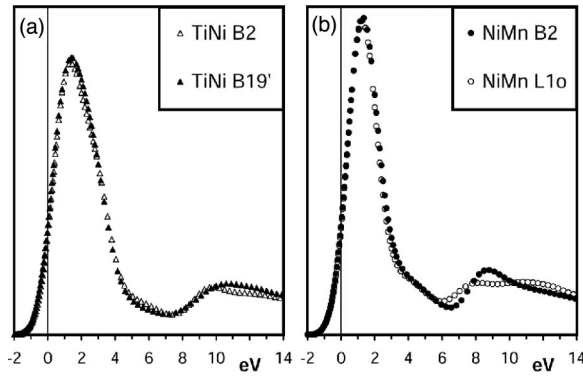


FIG. 5. Changes in the calculated Ni  $L_3$  EELS edges during (a) the  $B2 \rightarrow B19'$  transformation in TiNi and (b)  $B2 \rightarrow L1_0$  transformation in NiMn.

To address the problem of the ELNES dependence on the crystal structure, we have calculated the Ni  $L_3$  edges for different structural modifications of NiMn and TiNi. Although there is some difference in the DOS between  $B2$  TiNi and  $B19'$  TiNi [see Fig. 3(b)] the corresponding ELNES shapes are almost identical due to a loss of resolution [Fig. 5(a)]. In the case of NiMn [Fig. 5(b)],  $B2$  and  $L1_0$  show the same height and width of the white lines but different shapes for the secondary peaks. Nevertheless, the average position of the secondary peaks stays approximately the same in both structural modifications of NiMn.

#### IV. DISCUSSION

The changes in EELS spectra observed as a result of the formation of intermetallic compounds are commonly explained by changing chemical environments around the probed atoms while the effect of the crystal structure is ignored. The validity of such an approach has never been examined thoroughly because it is difficult to separate the structural and compositional effects on EELS, as most of the structural transformations in solids are accompanied by changes of chemical content. However,  $B2$  compounds such as TiNi and NiMn undergo martensitic, i.e., diffusionless transformations without changing the chemical composition, and therefore can be used as model systems for the study of the effect of the crystal structure on EELS. In agreement with earlier work by Murakami *et al.*,<sup>38</sup> we have not found any difference in the experimental ELNES of Ni and Ti atoms between the  $B2$  and  $B19'$  structures of TiNi. Calculations [Fig. 5(a)] indeed predict only a slight change in the Ni  $L_3$  profile upon the  $B2 \rightarrow B19'$  transformation, a change too small to be detected with the present experimental setup. These slight ELNES changes can be explained by a minor difference in interatomic distances between the  $B2$  and  $B19'$  modifications of TiNi,<sup>17,27</sup> leading to only a slight change in the actual shape of the DOS above  $E_F$  without shifting the peaks, as seen from Fig. 3(b). In principle, an improvement of the energy resolution can normally be achieved at the expense of a sharply reduced beam intensity, but this leads to poor statistics in the collection of ELNES. Moreover, the intrinsic broadening mechanisms arising from the finite life-

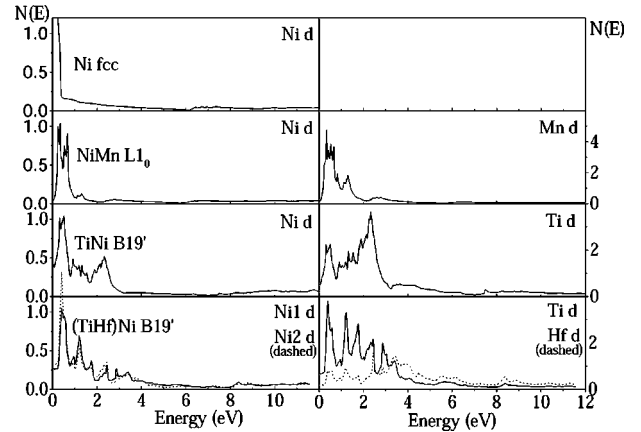


FIG. 6. Unoccupied density of states in different intermetallic compounds. Notice the correlation between  $d$  Ni and  $d$  TM states.

times of the initial and final excited states anyway limit the possibility of resolving fine-scale variations in the DOS near the Fermi level.

Even when severe differences are noted in the DOS between different structures, a clear distinction in the ELNES is not automatically guaranteed. One example is the case of the  $B2 \rightarrow L1_0$  transformation in NiMn. The coordination of Ni and Mn atoms and interatomic distances change more drastically than in TiNi, and, additionally, there is an antiferromagnetic ordering of the moments on Mn atoms in the  $L1_0$  NiMn structure. As a result, the  $B2 \rightarrow L1_0$  transformation in NiMn is accompanied by some significant DOS changes as seen in Fig. 3(b). The value of  $N(E_F)$  decreases by a factor of 20 [ $N(E_F) = 77.67$  electrons/cell/eV in  $B2$  and  $N(E_F) = 3.60$  electrons/cell/eV in  $L1_0$ ] while the peak located at  $E_F$  in the  $B2$  case shifts to a higher energy in  $L1_0$ . However, the changes of the shape of this peak above  $E_F$  result in a virtually unchanged integrated DOS in a window of 1 eV above  $E_F$ . Thus, the changes in the corresponding calculated EELS data are not so pronounced [Fig. 5(b)]. This is seen clearly when comparing the calculated partial Ni DOS [Fig. 3(b)] with Ni  $L_3$  ELNES [Fig. 5(b)] for  $B2$  and  $L1_0$  NiMn. Similar results were reported for the  $B2 \rightarrow 2H$  transformation in  $\text{Cu}_{70}\text{Al}_{27}\text{Ni}_3$ ,<sup>39</sup> i.e., no significant changes were observed in the ELNES, nor in experiments nor in calculations. It is thus concluded that an energy resolution of EELS around 1 eV is not sufficient to distinguish between structural modifications of intermetallic compounds.

In contrast, the effect of changing the chemical environments in most of cases can clearly be detected by EELS. As has been previously reported, the formation of the TM aluminides results in the splitting of the white lines in the TM  $L_{3,2}$  edges due to hybridization between the Al  $sp$  and TM  $d$  bands. In the present work, it was found that the formation of compounds between Ni and other TM's can cause a change in the width and shape of the white line as well as shifts of some of the fine ELNES features in the Ni  $L_{3,2}$  edge. The analysis of  $d$  partial DOS shows that these effects appear due to the hybridization between  $d$  Ni and  $d$  TM states. To illustrate this point, the calculated unoccupied  $d$  Ni DOS states are plotted in Fig. 6 in comparison with the corresponding

TM  $d$  DOS. In all intermetallic compounds, the positions of the local peaks of the Ni states coincide with the peaks of the  $d$  TM states over a large energy scale from  $E_F$  to  $E_F + 10$  eV. As was confirmed by varying the MT radii, such a feature is not an artifact of the calculations but implies a strong hybridization leading to common states between Ni and TM sites. We point out that all the observed ELNES changes can be fully explained in terms of  $d$  Ni– $d$  TM hybridization. In NiMn, the empty  $d$  Mn states are peaked just near  $E_F$ , thus  $d$  Ni– $d$  Mn hybridization does not result in the widening of the Ni  $L_3$  white line. In the case of TiNi, the empty  $d$  Ti states are spread far above  $E_F$ , and Ni-Ti hybridization gives a noticeable widening of the Ni  $L_3$  white line. In (TiHf)Ni, hybridization with the Hf band located at even higher energy than the Ti band gives an additional widening at the bottom of the Ni  $L_3$  white line.

Thus, in the investigated compounds, the chemical effect is clearly superior over the structural one. It is unclear at this point if this conclusion could be extended to the EELS study of defects, which might be considered as local changes of a crystal structure. In this case, the local changes of the bond lengths and coordination numbers can be more significant than those occurring during structural transformations, possibly causing some noticeable changes in the ELNES. Anyway, based on the present results, it is expected that the accuracy of EELS should be sufficient to detect the local changes of the chemical environment of the selected atoms due to nanoscale inhomogeneities or impurity segregation on defects.

Another problem frequently addressed in the literature is the charge transfer among atoms upon the formation of compounds. Based on *ab initio* calculations, many authors have reported a charge transfer usually directed from the element on the right-hand side of the periodic table to the element on the left-hand side.<sup>40–42</sup> However, it should be noted, as Muller *et al.*<sup>7</sup> cautioned against, that *ab initio* calculations cannot be used for arguments for the absence or presence of the charge transfer. As only charges within MT spheres around atoms are accounted for, the resulting numbers (even the direction of the transfer) depend crucially on the choice of the wave basis set and the size of the MT spheres. Thus, information about the charge transfer obtained from calculations should be only considered with reference to the MT radii used. In contrast, EELS provides a measurable quantity of the empty local DOS near the given atomic sites and is not affected by the conventions of computation. In this case, the probed area is defined by the overlap between the core and valence electronic waves and is constant for a given atom. The first accurate measurements of the Ni  $L$  cross sections in the Ni-Al system showed no significant difference in the number of  $d$  holes around a Ni atom among pure Ni, Ni<sub>3</sub>Al, and NiAl.<sup>7</sup> Based on this fact, Muller<sup>13</sup> assumed that the total charge around each atom did not change upon formation of compounds. This assumption, called “local charge neutrality,” is very important for the interpretation of EELS and allows the explicit connection between unoccupied DOS measured by EELS and occupied DOS, which are involved in the bonding. In the present work, taking into account the experimental precision, no change in the number of  $d$  holes

in NiAl when compared with pure Ni could be found (see Table I), which confirms Muller’s conclusions. Any possible charge transfer will thus be very small, and this is also supported by the results of calculations in Table II. The experimentally measured changes in the filling of the Ni  $d$  band on the formation of compounds with other TM’s [NiMn, TiNi, (TiHf)Ni, and Ti(NiCu)] were found to be negligible as well. In the case of the Cu  $d$  band, the absence of the white line in pure Cu and its appearance in Cu-containing compounds are often explained by the charge transfer from the Cu  $d$  band.<sup>11,45</sup> In the present work, the Cu white line was also observed in Ti(NiCu), but the quantitative analysis shows that in this case we deal with a sharp white line, which is formed by fusing a number of small peaks existing in pure Cu [see Fig. 1(d)], so again hardly any charge transfer will be present. We can roughly estimate the maximum value for possible charge transfer assuming that the valence  $3d$  band in pure Ni consists of 8.8 electron/atom<sup>44</sup> and therefore 1.2 hole/atom. From the values in the last column of Table I, this crude estimation yields a charge transfer from the Ni  $d$  band of about 0.1 electron/atom, which is even less than that estimated by Muller *et al.*<sup>7</sup> (0.2 electron/atom). Thus, the concept of local charge neutrality is shown to be reasonable for a wide range of intermetallic compounds.

As there is no significant charge transfer on the formation of intermetallic compounds, it is even less probable to expect it on structural transformations in these alloys. This conclusion does not confirm the results of Murakami *et al.*,<sup>38</sup> who reported a slight, but measurable charge transfer from a Ni atom to a Ti atom in the  $B2 \rightarrow B19'$  transformation in TiNi. In our own experiments, this result could not be reproduced, although the EELS data were obtained in the diffraction mode, which is a more quantitative method than the image mode used by Murakami *et al.*<sup>38</sup> Our calculations do show that a slight charge transfer may be expected from a Ni MT sphere, but the estimated value is so small that it can hardly be detected experimentally with the setups used in the present as well as earlier experiments.

## V. CONCLUSIONS

(1) The EELS simulations for the present intermetallic systems, based on the FLAPW DOS calculations, correspond well with the experimental data, including the fine ELNES details.

(2) The formation of intermetallic compounds between Ni and other transition metals causes measurable changes in the ELNES of the Ni  $L_{3,2}$  ionization edge. The observed changes can be successfully explained in terms of hybridization between the Ni  $d$  and the transition metal  $d$  bands.

(3) The structural transformations in the investigated Ni-containing intermetallics do not cause significant changes in the EELS spectra of the different elements. In all cases, the effect of the crystal structure on the EELS spectra is much smaller than the effect of chemical composition.

(4) The charge transfer on the formation of intermetallic compounds does not exceed 0.1 electron/atom. Thus, the concept of local charge neutrality is reasonable, which simplifies the interpretation of EELS spectra in metallic systems.

## ACKNOWLEDGMENTS

The authors wish to thank D.V. Valusky (ISPMS) for assistance in handling the programs. The useful discussion with G.A. Botton is gratefully acknowledged. One of the

authors (P.L.P.) acknowledges the financial support of the University of Antwerp, RUCA and the Interuniversity Poles of Attraction Program–Belgian State, Prime Minister’s Office–Federal Office for Scientific, Technical and Cultural Affairs (IUAP 4/10).

- <sup>1</sup>D. A. Muller, T. Sorch, S. Moccio, F. H. Baumann, K. Evans-Lutterodt, and G. Timp, *Nature (London)* **399**, 758 (1999).
- <sup>2</sup>D. A. Muller and M. J. Mills, *Mater. Sci. Eng., A* **260**, 12 (1999).
- <sup>3</sup>R. D. Leapman, L. A. Grunes, and P. L. Fejes, *Phys. Rev. B* **26**, 614 (1982).
- <sup>4</sup>D. H. Pearson, B. Fultz, and C. C. Ahn, *Appl. Phys. Lett.* **53**, 1405 (1988).
- <sup>5</sup>D. H. Pearson, C. C. Ahn, and B. Fultz, *Phys. Rev. B* **47**, 8471 (1993).
- <sup>6</sup>G. A. Botton, G. Y. Guo, W. M. Temmerman, and C. J. Humphreys, *Phys. Rev. B* **54**, 1682 (1996).
- <sup>7</sup>D. A. Muller, D. J. Singh, and J. Silcox, *Phys. Rev. B* **57**, 8181 (1998).
- <sup>8</sup>J. Zaanen, G. A. Sawatzky, J. Fink, W. Speier, and J. C. Fuggle, *Phys. Rev. B* **32**, 4905 (1985).
- <sup>9</sup>J. Fink, Th. Müller-Heinzerling, B. Scheerer, W. Speier, F. U. Hillebrecht, J. C. Fuggle, J. Zaanen, and G. A. Sawatzky, *Phys. Rev. B* **32**, 4899 (1985).
- <sup>10</sup>E. A. Stern and J. J. Rehr, *Phys. Rev. B* **27**, 3351 (1983).
- <sup>11</sup>G. A. Botton, G. Y. Guo, W. M. Temmerman, and C. J. Humphreys, in *Properties of Complex Inorganic Solids*, edited by A. Gonis, A. Meike, and P. Turchi (Plenum, New York, 1997), p. 175.
- <sup>12</sup>G. A. Botton and C. J. Humphreys, *Intermetallics* **7**, 829 (1999).
- <sup>13</sup>D. A. Muller, *Phys. Rev. B* **58**, 5989 (1998).
- <sup>14</sup>P. L. Potapov, A. V. Shelyakov, A. A. Gulyaev, E. L. Svistunova, N. M. Matveeva, and D. Hodgson, *Mater. Lett.* **32**, 247 (1997).
- <sup>15</sup>P. L. Potapov, A. V. Shelyakov, and D. Schryvers, *Scr. Mater.* **44**, 1 (2001).
- <sup>16</sup>E. Kren, E. Nagy, L. Pal, and P. J. Szabo, *J. Phys. Chem. Solids* **29**, 101 (1968).
- <sup>17</sup>G. M. Michal and R. Sinclair, *Acta Crystallogr., Sect. B: Struct. Crystallogr. Cryst. Chem.* **37**, 1803 (1981).
- <sup>18</sup>X. D. Han, W. H. Zou, R. Wang, Z. Zang, D. Z. Yang, and K. H. Wu, *J. Phys. (Paris), Colloq.* **5**, C8-753 (1995).
- <sup>19</sup>I. Baele, G. Van Tendeloo, and S. Amelinckx, *Acta Metall.* **35**, 401 (1987).
- <sup>20</sup>J. Taftø and O. L. Krivanek, *Nucl. Instrum. Methods Phys. Res.* **194**, 153 (1982).
- <sup>21</sup>R. F. Egerton and Z. L. Wang, *Ultramicroscopy* **32**, 137 (1990).
- <sup>22</sup>P. Blaha, K. Schwartz, and J. Luits, *WIEN 97* (Vienna University of Technology, Vienna, 1997), p. 161.
- <sup>23</sup>P. Blaha, K. Schwartz, P. Sorantin, and S. Trickey, *Comput. Phys. Commun.* **59**, 399 (1990).
- <sup>24</sup>M. Weinert, E. Wimmer, and A. J. Freeman, *Phys. Rev. B* **26**, 4571 (1982).
- <sup>25</sup>J. P. Perdew, S. Burke, and M. Ernzerhof, *Phys. Rev. Lett.* **77**, 3865 (1996).
- <sup>26</sup>P. L. Potapov, N. A. Poliakova, V. A. Udovenko, and E. L. Svistunova, *Z. Metallkd.* **87**, 33 (1996).
- <sup>27</sup>Y. Kudoh, M. Tokonami, S. Miyazaki, and K. Otsuka, *Acta Metall.* **11**, 2049 (1985).
- <sup>28</sup>H. Nam, T. Saburi, I. Nakata, and K. Shimizu, *Mater. Trans., JIM* **31**, 1050 (1990).
- <sup>29</sup>M. Nelhiebel, P.-H. Louf, P. Schattschneider, P. Blaha, K. Schwarz, and B. Jouffrey, *Phys. Rev. B* **59**, 12 807 (1999).
- <sup>30</sup>C. Hebert-Souche, P.-H. Louf, P. Blaha, M. Nelhiebel, J. Luitz, P. Schattschneider, K. Schwarz, and B. Jouffrey, *Ultramicroscopy* **83**, 9 (2000).
- <sup>31</sup>D. A. Muller, P. E. Batson, and J. Silcox, *Phys. Rev. B* **58**, 11 970 (1998).
- <sup>32</sup>J. E. Müller and J. W. Wilkins, *Phys. Rev. B* **29**, 4331 (1984).
- <sup>33</sup>R. D. Leapman, P. Rez, and D. F. Mayers, *J. Chem. Phys.* **72**, 1232 (1980).
- <sup>34</sup>C. C. Ahn and P. Rez, *Ultramicroscopy* **17**, 105 (1985).
- <sup>35</sup>E. J. Kirkland, Cornell University, Technical Report, 2000 (unpublished).
- <sup>36</sup>J. C. Fuggle, F. U. Hillebrecht, R. Zeller, Z. Zolnereck, and P. A. Bennett, *Phys. Rev. B* **27**, 2145 (1982).
- <sup>37</sup>P. Rez, J. R. Alvarez, and C. Pickard, *Ultramicroscopy* **78**, 175 (1999).
- <sup>38</sup>Y. Murakami, D. Shindo, K. Otsuka, and T. Oikawa, *J. Electron Microsc. J.* **47**, 301 (1998).
- <sup>39</sup>T. Hanada, R. Kitao, Y. Nakata, and Y. Hirotsu, in *European Conference on Electron Microscopy, Brno, 2000*, p. 1335.
- <sup>40</sup>A. Wegner, G. Buerri, and S. Steinemann, *Solid State Commun.* **9**, 1125 (1971).
- <sup>41</sup>V. L. Moruzzi, A. R. Williams, and J. F. Janak, *Phys. Rev. B* **10**, 4856 (1974).
- <sup>42</sup>K. Sham, *Phys. Rev. B* **31**, 1903 (1985).
- <sup>43</sup>D. Shindo, K. Hirada, A.-P. Tsai, and A. Chiba, *J. Electron Microsc. J.* **42**, 48 (1993).
- <sup>44</sup>L. Hodges, H. Ehrenreich, and N. M. Lang, *Phys. Rev.* **152**, 505 (1966).
- <sup>45</sup>0.574, as printed in the original paper, should be read 1.074, D. A. Muller (private communication).